Yidi WANG, Wei ZHENG

College of Aerospace and Material Engineering, National University of Defence Technology, Changsha 410073, China

Clock Error Control Algorithm for X-ray Pulsar-based Navigation Using a Single Detector

Abstract. The clock error control algorithm for X-ray pulsar-based navigation using a single detector is proposed. In this algorithm, the clock error on-board is also considered as a component of the explorer's state, and then it can be estimated during the navigation process. Moreover, an improved measurement model that uses both current and prior measurements is established. The comparison between two available measurement schemes is performed by the theory of nonlinear observability analysis. The result clearly shows that the explorer should sequentially measure different X-ray pulsars over the whole period of navigation for obtaining a desired performance. However, as compared to the multi-pulsar algorithm, the proposed algorithm suffers from loss of accuracy albeit to a magnitude tolerable for deep space navigation. The algorithm provides a prospective way for the realization of X-ray pulsar-based navigation.

Streszczenie. Zaprojektowano algorytm kontroli błędu zegara stosowanego w nawigacji w przestrzeni kosmicznej przy pomocy pulsara X (promieniowania rentgenowskiego) i pojedynczego detektora. W algorytmie błąd zegara pokładowego rozpatrzono jako składnik równań stanu statku kosmicznego, następnie przeprowadzono jego ocenę w procesie nawigacji. Ponadto przyjęto ulepszony model pomiarowy, wykorzystujący zarówno bieżące jak i poprzednie pomiary. Porównano dwa dostępne schematy pomiarowe, wykorzystując nieliniowe analizy obserwowalności. W pierwszym ze schematów, aby otrzymać satysfakcjonujące parametry nawigacji, statek może sekwencyjnie mierzyć różne pulsary X w całym okresie nawigacji. W porównaniu do algorytmu wielo-pulsarowego, proponowany w niniejszym opracowaniu algorytm daje mniejszą dokładność, chociaż wystarczającą do nawigacji w przestrzeni kosmicznej. Algorytm kontroli błędu zegara dla nawigacji opartej o pulsar promieniowania X, wykorzystujący jeden detektor

Keywords: X-ray pulsar-based navigation; Single detector; Clock error control
Słowa kluczowe: Nawigacja oparta o pulsar X; Pojedynczy detektor; Kontrola błędu zegara

Introduction

In the 21 century, the deep space mission has aroused global interests. Currently, the navigation and clock error control for the deep space explores are operated by the ground station systems [1]. However, the rapid development of the deep space mission puts increasingly heavy burdens on the ground station systems. Consequently, the autonomous navigation system using only the on-board measurement instruments is highly attractive [2].

The autonomous navigation for the deep space missions is mainly based on the line-of-sight measurement to stars combining measurements from a star sensor [3]. The method is self-contained but has poor performance because of the low-accuracy navigation sensors. Moreover, this method cannot correct or control the explorer's clock error that is one of the main error sources which worsen the performance of a navigation system.

X-ray pulsars are rapidly rotating neutron stars that provide unique and predictable pulse signals, and are extremely distant from the solar system [4]. Some X-ray pulsars have long term stabilities on the order of the current atomic clocks [5]. On other words, the X-ray pulsar-based navigation can estimate the position and velocity of the deep space explorer, and can control the clock error of the explorer.

However, in order to obtain a desired performance, the explorer was required to load at least three X-ray detectors with 1m² area [4]. Obviously, this is impractical for most explorers. Then, the idea of X-ray pulsar-based navigation observing a single pulsar was introduced. This method allows the explorer to load a single detector for navigation, but only one measurement is taken at a time. The method has poor observability [6]. Mao improved the method by fixing a gimballed axis under the single detector, and then the detector can be adjusted to sequentially receive the signals transmitted from different pulsars [7]. Although the performance and the observability of the method were improved Mao's work, the results were still not satisfactory. It is because that only the current measurement is used and measurements used are insufficient.

The objective of this paper is to derive a clock error control algorithm for X-ray pulsar-based navigation using a single detector. An improved measurement model that uses both current and prior measurements is established. Furthermore, based on the theory of nonlinear observability analysis, the condition number of the observability matrix is selected as a parameter to measure the observability8. If the condition number is great, the observability is poor because that the observability matrix is close to singular. The organization of the paper proceeds as follows. The improved navigation system is described in the following section. The comparison between two available measurement schemes is performed in Section 3. The simulation results are given in Section 4 and followed by Conclusions.

Improved navigation system
Dynamics model

The dynamics model of the explorer is composed of the trajectory dynamics model and the performance of the on-board atomic clock. The performance of the atomic clock can be described by a 3-state model driven by white noise. Let $\mathbf{E}_{clock}=[x_1, x_2, x_3]^T$ denote the clock error vector of the atomic clock, where x_1, x_2, x_3 denote the clock bias error, the clock drift error, and the clock drift rate error, respectively. In the sun centered coordinate system, the dynamics model can be described as [4]

$$(1) \quad \begin{bmatrix} \dot{\mathbf{r}} \\ \dot{\mathbf{v}} \\ \dot{\mathbf{E}}_{clock} \end{bmatrix} = \begin{bmatrix} \mathbf{v} \\ \mathbf{f} \\ \mathbf{d} \end{bmatrix} + \begin{bmatrix} \mathbf{w_r} \\ \mathbf{w_v} \\ \mathbf{w_E} \end{bmatrix}$$

where $\mathbf{X}=[\mathbf{r}^T, \mathbf{v}^T, \mathbf{E}_{clock}^T]^T$ is the state vector of the explorer, $\mathbf{d}$ equals $[x_2, x_3, 0]^T$, and $\begin{bmatrix} \mathbf{w_r}^T & \mathbf{w_v}^T & \mathbf{w_E}^T \end{bmatrix}^T$ is the process noise vector with covariance $\mathbf{Q}$ represented as

$$(2) \quad \mathbf{Q} = diag[q_r^2 \quad q_r^2 \quad q_r^2 \quad q_v^2 \quad q_v^2 \quad q_v^2 \quad q_1^2 \quad q_2^2 \quad q_3^2]$$

where q_r, q_v, q_1, q_2 and q_3 are the noise power spectral densities representing the position, velocity, clock bias error, clock drift error, and clock drift rate error, respectively.

In eq.(1), **f** is the force acting on the explorer and is defined as [8]

$$\text{(3)} \qquad \mathbf{f} = -\frac{\mu}{r^3}\mathbf{r} + \sum_{i=1}^{n_p} \mu_i \left(\frac{\mathbf{r}_{ri}}{r_{ri}^3} - \frac{\mathbf{r}_{pi}}{r_{pi}^3} \right) + \Delta\mathbf{F}$$

where n_p is the number of perturbation celestial bodies; r_{ri} is the position vector of the explorer with respect to the ith perturbation celestial body; r_{pi} is the position vector of the ith perturbation celestial body with respect to the Sun; μ is the gravitational coefficient of the Sun; μ_i is the gravitational coefficient of the ith perturbation celestial body; and $\Delta\mathbf{F}$ stands for the other perturbation forces including the effects of solar radiation pressure and non-spherical perturbation of the Sun.

Improved measurement model

The fundamental measurement of the X-ray pulsar-based navigation is the difference between the pulse time-of-arrival (TOA) at the explorer, $t_{S/C}$, and the corresponding pulse TOA at the solar system barycenter (SSB), $\tilde{t}_{SSB}$. $t_{S/C}$ can be obtained after a period of measurement, and $\tilde{t}_{SSB}$ can be predicted by the pulsar pulse-timing model [4].

Considering the relativistic and geometric effects, $t_{S/C}$ can be transferred to its coordinate time at the SSB, t_{SSB}, by using the following equation [4]

$$
\begin{aligned}
\text{(4)} \qquad t_{SSB} = t_{S/C} &+ \frac{\mathbf{n}\cdot(\mathbf{r}+\mathbf{b})}{c} \\
&+ \frac{1}{2cD_0}\left[\begin{array}{l} (\mathbf{n}\cdot(\mathbf{r}+\mathbf{b}))^2 - (\mathbf{r}+\mathbf{b})^2 \\ +2(\mathbf{n}\cdot\mathbf{b})(\mathbf{n}\cdot(\mathbf{r}+\mathbf{b})) - 2(\mathbf{b}\cdot(\mathbf{r}+\mathbf{b})) \end{array} \right] \\
&+ \frac{2\mu}{c^3}\ln\left| \frac{\mathbf{n}\cdot(\mathbf{r}+2\mathbf{b}) + \|\mathbf{r}+2\mathbf{b}\|}{\mathbf{n}\cdot\mathbf{b}+b} \right|
\end{aligned}
$$

In eq.(4), **n** is the unit direction vector of the pulsar with respect to the SSB; c is the speed of light; D_0 is the distance between the SSB and the pulsar; and **b** is the position vector of the Sun with respect to the SSB. The second term on the right hand side of eq.(4) is the first-order Doppler delay, the third term is due to the effect of annual parallax, and the fourth term is the Shapiro delay effect.

r and $t_{S/C}$ can be expressed as

$$
\begin{aligned}
\text{(5)} \qquad & \mathbf{r} = \tilde{\mathbf{r}} + \delta\mathbf{r} \\
& t_{S/C} = \tilde{t}_{S/C} + \delta t_{S/C}
\end{aligned}
$$

where $\tilde{\mathbf{r}}$ is the real position vector of explorer; $\delta\mathbf{r}$ is the position offset; $\tilde{t}_{S/C}$ is the real pulse TOA at the explorer; and $\delta t_{S/C}$ is the clock error. According to eq.(4), $\tilde{t}_{SSB}$ can be rewritten as

$$
\begin{aligned}
\text{(6)} \qquad \tilde{t}_{SSB} = \tilde{t}_{S/C} &+ \frac{\mathbf{n}\cdot(\tilde{\mathbf{r}}+\mathbf{b})}{c} \\
&+ \frac{1}{2cD_0}\left[\begin{array}{l} (\mathbf{n}\cdot(\tilde{\mathbf{r}}+\mathbf{b}))^2 - (\tilde{\mathbf{r}}+\mathbf{b})^2 \\ +2(\mathbf{n}\cdot\mathbf{b})(\mathbf{n}\cdot(\tilde{\mathbf{r}}+\mathbf{b})) - 2(\mathbf{b}\cdot(\tilde{\mathbf{r}}+\mathbf{b})) \end{array} \right] \\
&+ \frac{2\mu}{c^3}\ln\left| \frac{\mathbf{n}\cdot(\tilde{\mathbf{r}}+2\mathbf{b}) + \|\tilde{\mathbf{r}}+2\mathbf{b}\|}{\mathbf{n}\cdot\mathbf{b}+b} \right|
\end{aligned}
$$

Then the difference between t_{SSB} and $\tilde{t}_{SSB}$ is

$$\text{(7)} \qquad \delta t = t_{SSB} - \tilde{t}_{SSB} = \frac{\mathbf{n}\cdot\delta\mathbf{r}}{c} + \delta t_{S/C} + \delta t'_1 + \delta t'_2$$

Compared with the first and the second terms on the right hand side of eq.(7), the third and the fourth terms on the right hand of eq.(7) are high-order terms that can be neglected.

Then, the measurement model can be presented as

$$
\begin{aligned}
\text{(8)} \qquad & \delta t = \mathbf{N}\delta\mathbf{X} + \mathbf{v} \\
& \mathbf{N} = [\mathbf{n}/c \quad \mathbf{0}_{1\times3} \quad 1 \quad 0 \quad 0]
\end{aligned}
$$

where **n** equals $[n_x \ n_y \ n_z]$; $\delta\mathbf{X}$ is the state offset of the explorer; **N** is the measurement matrix; and **v** is the zero-mean Gaussian white noise with standard variance σ_{TOA} given by [9]

$$\text{(9)} \qquad \sigma_{TOA} = \frac{\sqrt{\frac{1}{4}T_{50}^2 + T_b^2}}{\sqrt{A\cdot t_m}} \cdot \frac{\sqrt{\lambda_n + \lambda_p}}{\lambda_p}$$

where λ_p and λ_n are the average flux of pulsar signal and the average background radiation flux, respectively; A is the effective area of the detector; t_m is the period of measurement; T_{50} is the width of pulse; and T_b is the timing error of any individual photon detected by the detector onboard.

From the theory of trajectory dynamics, $\delta\mathbf{X}$ at time t_j can be expressed as [9]

$$\text{(10)} \qquad \delta\mathbf{X}_j = \mathbf{\Phi}(t_j, t_k)\delta\mathbf{X}_k$$

where $\delta\mathbf{X}_k$ is the state offset of the explorer at time t_k, and $\mathbf{\Phi}(t_j, t_k)$ is the transition matrix between time t_j and time t_k. It follows from eqs.(8) and (10) that the measurement at time t_j can be written as

$$\text{(11)} \qquad \delta t_j = \mathbf{N}_j\mathbf{\Phi}(t_j, t_k)\delta\mathbf{X}_k + v_j$$

where N_j is the measurement matrix during the jth period of measurement, and v_j is the measurement noise at time t_j.

At the kth navigation time, t_k, it follows from eq.(11) that the improved measurement model can be established as

$$\text{(12)} \qquad \mathbf{Z} = \mathbf{H}\delta\mathbf{X}_k + \mathbf{V}$$

where

$$\text{(13)} \quad \mathbf{Z} = \begin{bmatrix} \delta t_{k-i+1} \\ \vdots \\ \delta t_{k-1} \\ \delta t_k \end{bmatrix}, \mathbf{H} = \begin{bmatrix} \mathbf{N}_{k-i+1}\mathbf{\Phi}(t_{k-i+1}, t_k) \\ \vdots \\ \mathbf{N}_{k-1}\mathbf{\Phi}(t_{k-1}, t_k) \\ \mathbf{N}_k \end{bmatrix}, \mathbf{V} = \begin{bmatrix} v_{k-i+1} \\ \vdots \\ v_{k-1} \\ v_k \end{bmatrix}$$

where δt_k, δt_{k-1},..., δt_{k-i+1} are the current and prior measurements; $\mathbf{N}_k$, $\mathbf{N}_{k-1}$, ..., $\mathbf{N}_{k-i+1}$ are those measurement matrices during the kth, k–1th, ..., k–i+1th period of measurement respectively; $\mathbf{\Phi}(t_{k-1}, t_k)$, ..., $\mathbf{\Phi}(t_{k-i+1}, t_k)$ are transition matrices; v_k, v_{k-1}, ..., v_{k-i+1} are the measurement noise at times $t_k, t_{k-1},..., t_{k-i+1}$ respectively.

Compared with the previous measurement models that used only the current measurement, the improved measurement model can use both current and prior measurements. Then, by using the improved measurement model, the explorer can use at least three measurements at a time once the third navigation time has passed. In other words, the improved measurement model would ensure that the explorer uses enough measurements.

Measurement scheme comparison

Obviously, the improved navigation system proposed above is a nonlinear system. The observability of the system can be investigated from a differential geometric point of view. The observability investigation considers the following system:

$$\text{(14)} \qquad \begin{cases} \dot{\mathbf{X}} = f(\mathbf{X}) \\ \mathbf{Z} = h(\mathbf{X}) \end{cases}$$

The system in eq.(14) is weakly observable around the reference point X_0, if and only if the observability matrix defined as

$$\text{(15)} \qquad \mathbf{O} = \begin{bmatrix} dL_f^0 h(\mathbf{X}) \\ dL_f^1 h(\mathbf{X}) \\ \vdots \\ dL_f^{n-1} h(\mathbf{X}) \end{bmatrix}$$

has full column rank [10].

In eq.(15), n is the order of $\mathbf{X}$ (for this system, n = 9) and $dL_f^k h(\mathbf{X})$ is

$$(16) \qquad dL_f^k h(\mathbf{X}) = \frac{\partial(L_f^k h)}{\partial \mathbf{X}}, k = 0, 1, \cdots, n-1$$

where $L_f^k f(\mathbf{X})$ is

$$(17) \qquad \begin{cases} L_f^0 h(\mathbf{X}) = h(\mathbf{X}) \\ L_f^k h(\mathbf{X}) = \dfrac{\partial(L_f^{k-1} h)}{\partial \mathbf{X}} f(\mathbf{X}), k = 0, 1, \cdots, n-1 \end{cases}$$

The condition number of the observability matrix in eq.(15) can be used to measure the observability. It is useful to compare the performance of different measurement schemes. If the condition number is great, the observability is poor because the observability matrix is close to singular.

There are two measurement schemes that need to be compared. In scheme I, the explorer measures a single pulsar over the whole period of navigation. In scheme II, the explorer sequentially measures three pulsars over the whole period of navigation.

In order to illustrate the comparison, a family of Sun-centered orbits is chosen. The orbital elements of the orbits are shown in Table.1. Each period of measurement is 2 hours, and the number of measurement times is 300s.

Table 1. Orbital elements of the family of Sun-centered orbits

Orbital Element	a/10^8 km	e	i/°	Ω/°	ω/°	M/°
Values	[0.5, 2]	[0,0.5]	1.922	0	297.9	0

Fig.1 shows the condition numbers for varying values between a and e by using scheme I. It is shown that the condition number increases as a increases and decreases as e increases. On the one hand, the increment of a slows down the mean velocity of the orbit and results in transition matrices appearing more similar. Then, the condition number of the observability matrix becomes larger. On the other hand, the increment of e sharpens the orbit and results in transition matrices appearing more different.
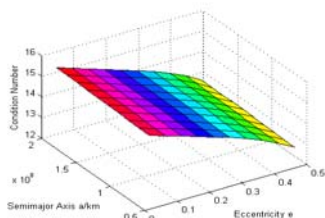
Fig.1. Condition numbers between semi-major axis and eccentricity for scheme I
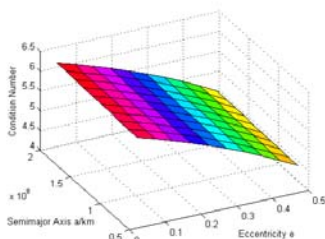
Fig.2. Condition numbers between semi-major axis and eccentricity for scheme II

Fig.2 shows the condition number for varying values between a and e by using scheme II. As compared with scheme I, the condition numbers obtained by using scheme II are smaller for the reason that the row vectors composing the observability matrix tend to be linearly independent by introducing different direction vectors of pulsars into the matrix. Therefore, the explorer should sequentially measure different X-ray pulsars over the whole period of navigation.

Simulation and discussion
In order to verify the feasibility and effectiveness of the proposed algorithm, a comparison is made against multi-detector algorithm. The simulations of scheme I and scheme II are also given to verify the conclusion obtained in Section 3.

Table 2 shows the elements of explorer orbit. The X-ray pulsars PSR B1937+21, PSR B1957+20, and PSR J0218+4232 are used in scheme II. In scheme I, only the PSR B1957+20 is used. The parameters of these X-ray pulsars are given in Table 3. The position error of the pulsars is 0.1mas. The effective area of the onboard detector is 1m^2, and the timing error of any individual photon is 1μs.

The UKF is selected as the navigation filter with the beginning position error [10km, 10km, 10km], beginning velocity error [10m/s, 10m/s, 10m/s], and beginning clock error vector [3.5858×10^{-6}s, 3.637979×10^{-11}, 6.66×10^{-18}s^{-1}]. q_r, q_v, q_1, q_2, and q_3 in eq.(2) are 0.01, 0.0001, 1.11×10^{-22}s, 2.22×10^{-32}/s, and 6.66×10^{-45}/s^3, respectively. The period of navigation is 50days, and the period of measurement is 2 hours.

Table.2. Elements of explorer orbit

Orbital Element	a/km	e	i/°	Ω/°	ω/°	M/°
Values	194618992	0.1	0.12	184.52	121.2	327.1

Table.3. Parameters of the pulsars used in simulation

X-ray pulsars	Galactic longitude/°	Galactic latitude/°	Period /ms
PSR B1937+21	57.51	-0.29	1.56
PSR B1957+20	59.20	-4.70	1.60
PSR J0218+4232	139.51	-17.53	2.32

Fig.3. shows the estimation errors of the position and clock error by using Scheme I, and Fig.4 shows the estimation errors of the position and clock error by using Scheme II.
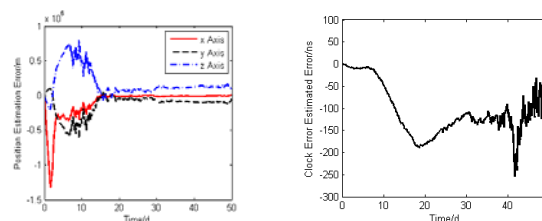
(a) Position estimation error (b) Clock error estimation error
Fig.3.Navigation results by using scheme I
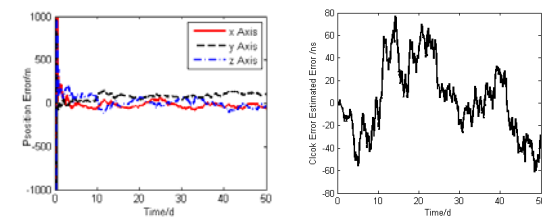
(a) Position estimation error (b) Clock error estimation error
Fig.4.Navigation results by using scheme II

As are illustrated in Fig.3 and Fig.4, the curves of the position estimation error converges gradually by using scheme I or scheme II. In terms of convergence performance, the scheme II is quite better than scheme I. Moreover, the curve of clock error estimation error would

diverge by using scheme I, but it could converge by using scheme II. It verifies the conclusion obtained in Section 3.

Table 4 gives the average values of position estimation errors and clock error estimation errors (1σ) over 300 Monte-Carle trails. It is learnt that the performance of the proposed algorithm is not better than the multi-detector algorithm and suffers from loss of accuracy albeit to a magnitude tolerable for deep space navigation.

Table.4. Comparison between the performances of two algorithms

	Proposed algorithm	Multi-detector algorithm
Positioning Accuracy/m	249.46	228.99
Timing Accuracy/ns	81.75	80.56

Conclusion

The clock error control algorithm for X-ray pulsar-based navigation using a single detector has been proposed. In this algorithm, both the current and the prior measurements are used for navigation. As compared to multi-detector algorithm, the proposed algorithm suffers from loss of accuracy albeit to a magnitude tolerable for deep space navigation. It is shown that the explorer should sequentially measure different pulsars for obtaining a desired navigation performance. Moreover, this algorithm uses a single X-ray detector, and helps to reduce the cost and the whole mass of the navigation system. The algorithm provides a prospective way for the realization of X-ray pulsar-based navigation.

REFERENCES
[1] H.B.Wiliam. Deep Impact Mission Design. *Space Science Reviews*, 2 (2005) 23-42.
[2] K.H. Glassmeier, H.Boehnhardt, D.Koschny. Flying towards the origin of the solar system. *Space Science Reviews*, 2 (2007) 1-21.
[3] Jo Ryeong Yim, John L. Crassidis and John L. Junkins. Autonomous Spacecraft Orbit Navigation of Interplanetary Spacecraft. *Proceeding of AIAA Guidance, Navigation, and Control Conference*, USA: Denver, (2000) 53-61.
[4] Suneel Ismail Sheikh. The Use of Variable Celestial X-Ray Sources for Spacecraft Navigation. *Doctoral Dissertation*, University of Maryland, (2005).
[5] A. Robert Golshan, Suneel I. Sheikh, On Pulse Phase Estimation and Tracking of Variable Celestial X-Ray Sources. *ION 63rd Annual Meeting*, England: Cambridge, (2007) 413-422.
[6] Zheng Guanglou. Liu jianye, Qiao Li et al. Observability Analysis of Satellite Autonomous Navigation System Using Single Pulsar. *Journal of Applied Sciences-Electronics and Information Engineering (in Chinese)*, 5 (2008) 506-510.
[7] Mao yue, Chen jianpeng, Song xiaoyong. Single X-ray Pulsar Dynamic Orbit Determination. *Journal of Geomantics Science and Technology*, 4 (2010) 251-254.
[8] Battin,R.H. *An Introduction to the Mathematics and Methods of Astrodynamics*. New York Willey (1999).
[9] Dennis W. Woodfork. The use of X-Ray pulsars for aiding GPS satellite orbit determination. *Master Dissertation*, Air Force Institute of Technology, 2005.
[10] Herman R, and Krener A. K. Nonlinear Controllability and Observability, *IEEE transactions on autonomous control*, 5 (1977) 728-740.

Authors: Doctor wang yidi; Prof. Zheng Wei, College of Aerospace and Material Engineering, National University of Defence Technology, Changsha 410073, China, E-mail: *zhengwei@nudt.edu.cn*